IEEE Access
Multidisciplinary ⋮ Rapid Review ⋮ Open Access Journal

Received March 29, 2022, accepted April 5, 2022, date of publication April 8, 2022, date of current version May 26, 2022.

Digital Object Identifier 10.1109/ACCESS.2022.3165815

Hybrid Entropy in the Time-Frequency Domain for Grading Electrode Sediment Identification

WEIHUA CHEN[1], HONGQIANG CHEN[1], XIAOHENG YAN[1], YANJU YANG[2], AND SHIWEI JIN[3]

[1]Faculty of Electrical and Control Engineering, Liaoning Technical University, Huludao 125105, China
[2]School of Electronic Information and Electrical Engineering, Chongqing University of Arts and Sciences, Chongqing 402160, China
[3]State Grid Liaoning Maintenance Company, Shenyang 110003, China

Corresponding author: Xiaoheng Yan (xiaohengyan@163.com)

This work was supported in part by the Scientific and Technological Research and Innovation Team Project of Liaoning Provincial Department of Education under Grant LT201900, and in part by the Science and Technology Project of State Grid Corporation of China under Grant SGLNJX00YJJS2100620.

ABSTRACT The traditional manual periodic screening method of grading electrode sediments is prone to cause the equipment failure of high voltage direct current converter valves. Therefore, we propose to use ultrasonic time-domain reflection method to detect the sediments. However, the ultrasonic echo signals are characterized by nonlinearity and nonsmoothness, which makes it very difficult to extract effective features for sediment detection. To address this issue, we propose an intelligent detection method based on multiscale hybrid entropy characteristics in the time-frequency domain. First, a multiscale decomposition of the signal is performed. Second, the weighted form factor index is proposed to select the noise modes. Moreover, we propose to calculate the hybrid entropy in the time-frequency domain of each mode as the characteristic input bidirectional long and short-term memory network model, and verified that feature enhancement can be achieved by noise modes noise reduction. Finally, the experimental validation shows that the proposed method can achieve nondestructive testing and intelligent identification of graded electrode sediment with a correct identification rate of 94.25%.

INDEX TERMS Electrodes, electrical fault detection, entropy, feature extraction, neural networks, nondestructive testing, noise reduction, sediments, signal detection, signal processing.

I. INTRODUCTION

Grading electrodes are key devices for mitigating electrolytic corrosion in the cooling system of high voltage direct current (HVDC) converter valves. As cooling system radiator corrosion leads to sediment deposition on grading electrodes, the breakage and falling of sediments lead to pipeline blockage, equipment overheating and other problems, causing a threat to the safe operation of the HVDC converter valve equipment [1]–[3]. For this reason, researchers have investigated the mechanism of sediment deposition on grading electrodes. Wang *et al.* [4] investigated the mechanism of sediment deposition on grading electrodes in cooling water dielectric of high voltage (HV) converter valve and the method of suppression. Song *et al.* [5] proposed an electrochemical diffusion coupling model to study the sediment deposition behaviour on the electrode surface. The results indicated that the maximum sediment thickness and concentration are occurred in the tip section of electrode surface. Wang *et al.* [6] investigated the distributing characteristics of sediment deposited on pin-type grading electrodes in Inner cooling circuit of HV converter valve and indicated that the deposition degree of the sediment is mainly dominated by the electrical current through the pin-type grading electrode. Yang *et al.* [7] investigated the phenomenon and mechanism of deposition on platinum electrodes in HVDC converter valves, and indicated through simulation experiments and numerical calculations that the deposited sediment on the platinum electrode is rod-shaped and that the growth rate of sediment thickness decreases with time. However, the above studies did not investigate the detection and identification of sediment at the grading electrodes. Therefore, the detection of sediment at the grading electrodes is the key to the research of this paper. At present, the method of manually screening the electrodes individually is mainly used to observe the sediment condition of the grading electrode. This traditional method easily causes equipment leakage due to disassembly and reassembly of pipes,

The associate editor coordinating the review of this manuscript and approving it for publication was Gerard-Andre Capolino.

which leads to problems such as equipment short circuits. To achieve nondestructive detection of pipe defects, numerous studies have focused on the use of electromagnetic acoustic transducers (EMATs) [8], circumferential Lamb waves [9], and ultrasonic guided waves [10]. However, the above methods can only detect defects on or near the surface of the workpiece, and are no longer applicable to the inspection of grading electrodes located inside composite pipes. For the detection of sediment in pipes, many scholars have used ultrasonic time-domain reflectometry (UTDR) to obtain sediment echo signals for quantitative analysis [11]–[14]. This method enables fixed-point detection of the object under test [15], [16]. Therefore, it meets the requirements of grading electrode sediment detection. However, the method requires the inspectors to further identify the sediment condition based on the sediment echo vibration characteristics and discriminative experience, and problems such as unclear signal characterization and manual misdetection as well as inspection misses. Intelligent identification and detection of sediment signals are not achieved. Moreover, the sediment echo signal is nonlinear and nonsmooth in nature, and is easily disturbed by noise, thus increasing the difficulty of sediment echo signal feature extraction and identification. Therefore, effective characterization of the features of the sediment echo signal under noise interference is key to realizing intelligent identification of the sediment condition of the grading electrode.

To extract effective features of nonstationary signals, the traditional statistical properties in the time and frequency domains cannot meet the requirements, but entropy theory can be introduced to effectively evaluate the complexity and irregularity of the signal [17]–[19]. Entropy-based methods have been introduced to nondestructive testing (NDT) and diagnosis, including approximate entropy [20], sample entropy [21], fuzzy entropy [22], and multiscale entropy [23]. Due to the attenuation characteristics of ultrasonic waves during propagation, the echo signal shows amplitude and energy attenuation phenomena [24]–[26], so the degree of grading the electrode sediment can be assessed by extracting the entropic features reflecting the changes in signal amplitude and energy. Azami *et al.* [27] proposed fluctuation-based dispersion entropy (FDE) on the basis of dispersion entropy, which takes into account the differences in the dispersion patterns of neighbouring units and fully considers the variation between amplitudes from the time-domain perspective to avoid the loss of useful amplitude information. Ke *et al.* [28] proposed a hierarchical fluctuation dispersion entropy to measure the internal dynamics of the signal based on the fluctuation-based dispersion entropy and verified the effectiveness of the method in common rail injector fault feature extraction. Li *et al.* [29] defined the Hilbert marginal spectrum energy entropy(HMSEE) based on the Hilbert marginal spectrum using the concept of entropy, which can be used to effectively characterize the amplitude change of the signal at an instantaneous frequency from the frequency domain perspective. Yang *et al.* [30] extracted the Hilbert marginal spectral energy entropy as a feature vector to assess the mechanical fault state of circuit breakers in power systems and showed the effectiveness of the proposed method. However, the above studies only extract the entropy features of the signal from a single perspective in the time domain or frequency domain, and does not consider both the time and frequency domains simultaneously, which results in inadequate signal characterization. Therefore, we propose to use the fluctuation-based dispersion entropy and Hilbert marginal spectral energy entropy to form a hybrid entropy as features to achieve adequate extraction of signal features from both time and frequency domains.

Moreover, most of the above studies use limited single-scale analysis, ignoring the information embedded in the multiscale features of the signal, which is prone to the loss of fault information. In view of the above facts, Costa *et al.* [31] and Aziz *et al.* [32] introduced multiscale entropy (MSE) and multiscale replacement entropy (MPE), respectively, to assess the irregularity of time series and overcome the drawbacks of entropy-based estimation methods that consider only a single scale. Many scholars use empirical mode decomposition (EMD) to perform multiscale decomposition of signals by extracting the entropy values of different scales of modes as the feature vectors for fault diagnosis. Ji *et al.* [33] proposed an empirical mode decomposition-refined composite multiscale dispersion entropy analysis (EMD-RCMDEA) and verified the validity and stability of the method. Xie *et al.* [34] proposed to apply EMD to decompose the signal and extract the entropy of the effective modes as features for fatigue and fault pattern recognition of fan blades. However, EMD is prone to the phenomenon of mode confusion during the decomposition process. Based on this, variational mode decomposition (VMD) can be used to efficiently decompose the nonstationary signal into intrinsic mode functions (IMFs) of different scales [35] and overcome the flaws of the EMD method; its advantages in dealing with nonsmooth signals have been demonstrated in previous studies. Ni *et al.* [36] proposed a fault information-guided VMD (FIVMD) method for extracting the weak bearing repetitive transient and proposed the ratio of fault characteristic amplitude (RFCA) to optimize the VMD decomposition parameters. Huang *et al.* [37] proposed to analyze the acoustic signal of defects inside an arc magnet using a combination of variational mode decomposition and beetle antennae search, and proposed to optimize the VMD parameters using beetle antenna search. Liu *et al.* [38] proposed a signal analysis method combining variational modal decomposition and detrended fluctuation analysis (DFA), and proposed a simple criterion based on DFA to select the number of modes. In this paper we achieve the optimization of VMD performance by determining the number of modes based on a simple criterion of the centre frequency method.

After decomposing the signal into different scale modes using VMD, filtering out the noise modes is key to achieving signal noise reduction and feature enhancement. In [39], [40], the authors used the correlation coefficient method for noise mode selection, but the conventional correlation coefficient

method is vulnerable to noise interference, and a single indicator does not fully interpret the fluctuating characteristics of the signal, making it is less effective in distinguishing noise modes. In [41], [42], the authors applied the weighted kurtosis index for noise mode selection of vibration shock signals, since the WKI takes into account the advantage of the high sensitivity of the kurtosis index to the shock component of the vibration signal, the combination of the correlation coefficient and the kurtosis index improves the accuracy of the noise mode screening of the vibration shock signal. However, this criterion is not sensitive to changes in the amplitude distribution of the ultrasonic echo signal and may ignore some components with large amplitudes and scattered distributions. Therefore, we propose a new method of weighted form factor index (WFF) to filter out the noise modes of ultrasound signals.

To solve the above problems, this paper proposes an intelligent identification method of grading electrode sediment based on multiscale hybrid entropy in the time-frequency domain, as the identification of grading electrode sediment is a new topic. The contributions of this paper can be summarized as follows.

1) We propose to use ultrasonic time domain reflection method to achieve the first nondestructive detection of sediment of the grading electrode. Thus, we obtained the signal data of the grading electrode sediment.

2) We propose a new method of weighted form factor index (WFF), which effectively filter out the noise modes of ultrasonic echo signals and solves the problem of difficult selection of noise modes of ultrasonic echo signals.

3) We propose to calculate the fluctuation-based dispersion entropy and Hilbert marginal spectral energy entropy of each mode to form hybrid entropy (HE) in the time-frequency domain as the feature vector, which realizes the full extraction of signal features from the time-frequency domain. And the feature vector is input into a bidirectional long and short-term memory (Bi-LSTM) network model to achieve the recognition of graded electrodes with different sediment thicknesses, verifying that the recognition rate of entropy values based on the time-frequency domain is better than the entropy value in the time or frequency domains alone.

4) We propose an improved wavelet threshold function. On the basis of noise reduction of the noise modes, the enhancement of the entropy value feature is achieved, which in turn improves the recognition accuracy.

The paper is organized as follows: Section 2 details the research methodology and the proposed work. Section 3 presents the experimental validation and analysis of the results. Section 4 summarizes the conclusions.

II. MATERIALS AND METHODS

A. MECHANISM OF GRADING ELECTRODE SEDIMENT DEVELOPMENT

To avoid damage to the components in the converter valve caused by overheating, deionized water is used as the coolant for the valve cooling system. Although the deionized water has low conductivity, the generation of leakage current is inevitable due to the relatively big potential difference of the metal components the coolant flows over, resulting in corrosion of metal components. Generally, grading electrodes are installed in the cooling system to reduce corrosion. However, ions generated by the corrosion of aluminum radiators move to the surface of the grading electrodes and produce sediment by electrochemical reactions. Under certain conditions, the surface of aluminum radiators can undergo electrochemical reactions in water as follows.

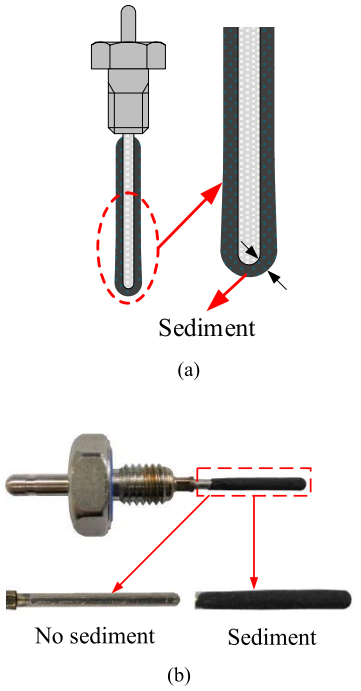

FIGURE 1. Distribution of sediment at the graded electrode: (a) indicates the area at the tip of the graded electrode where the thickness of the sediment layer is larger, and (b) indicates the sample appearance of the actual grading electrode after the presence of sediment, the main component of the sediment is $Al(OH)_3$.

$$2Al \rightarrow 2Al^{3+} + 6e^{-} \quad (1)$$

$$6H_2O \rightarrow 6H^{+} + 6OH^{-} \quad (2)$$

$$6H^{+} + 6e^{-} \rightarrow 3H_2 \uparrow \quad (3)$$

$$2Al^{3+} + 6OH^{-} \rightarrow 2Al(OH)_3 \downarrow \quad (4)$$

As is shown in Figure 1, the sediment adheres to the surface of the grading electrode, the main component of the sediment is $Al(OH)_3$, and the thickness of the sediment layer is larger on the area of the tip of the grading electrode [7]. After deposition of the sediment layer on the surface of the grading electrode, the sediment thickness can reach up to 0.3-0.8 mm [43]. At present, the method of shutting down the converter valve and sampling the electrode to observe the degree of sediment is typically adopted, which has relatively large blindness and easily leads to water leakage. Therefore, a new method is needed for online inspection of the sediment status of the grading electrode.

B. MULTISCALE DECOMPOSITION AND ENTROPY FEATURE ENHANCEMENT OF ULTRASONIC ECHO SIGNALS

Single-scale features cannot effectively characterize the rich information of ultrasonic signals. To reflect the characteristics of the signal at different scales, the multiscale decomposition of the signal is performed by using variational modal decomposition.

The process of variational modal decomposition can be converted into the construction and solution of variational models. The constrained variational model of the modal component is

$$\begin{cases} \min\limits_{\{u_k\},\{\omega_k\}} = \left\{ \sum\limits_k \left\| \partial_t \left[\left(\delta(t) + \dfrac{j}{\pi t} \right) u_k(t) \right] e^{-j\omega_k t} \right\|_2^2 \right\} \\ s.t. \sum\limits_k u_k = f \end{cases} \tag{5}$$

where f is the original input signal; k is the number of modes; u_k denotes the mode obtained by decomposition; and ω_k denotes the centre frequency of each mode. To solve Equation (5), the constrained variational model in Equation (5) can be converted to an unconstrained variational model before applying the alternating direction multiplier algorithm. Finally, the optimal solution of Equation (5) is obtained by iteratively updating the centre frequency and bandwidth of each mode component, thus realizing the adaptive decomposition of the signal.

To reduce the influence of noise modes on entropy feature extraction, the noise modes need to be screened out for noise reduction and to realize the enhancement of entropy features. The commonly used correlation coefficient method is relatively onefold and vulnerable to noise interference as an evaluation index, and cannot effectively screen out the noise modes of the ultrasonic echo signal. In contrast, the form factor, as a dimensionless statistic in the time domain signal, is sensitive to the variation and fullness of the signal waveform amplitude. Therefore, combining these two indicators can improve the sensitivity to the effective mode components and better screen out the noise modes. Since the correlation coefficient satisfies $|C| \leq 1$, the correlation coefficient is used to weight the form factor, and a new evaluation index, the weighted form factor (WFF) index, is proposed, which is defined as follows:

$$WFF = F \cdot C \tag{6}$$

$$F = \frac{\sqrt{\frac{1}{N}\sum\limits_{n=1}^{N} u_k^2}}{\frac{1}{N}\sum\limits_{n=1}^{N} |u_k|} \tag{7}$$

$$C = \frac{\sum\limits_{n=1}^{N} (u_k - \bar{u}_k)(x - \bar{x})}{\sqrt{\sum\limits_{n=1}^{N} (u_k - \bar{u}_k)^2 \sum\limits_{n=1}^{N} (x - \bar{x})^2}} \tag{8}$$

where F, C are the form factor and correlation coefficient, respectively; x and $\bar{x}$ are the signal sample value and its mean value respectively; u_k and $\bar{u}_k$ are the kth IMF and its mean value respectively; and N is the number of echo signal sampling points. If the weighted form factor index calculated by Equation (6) is greater than 1, it is considered as a valid mode, otherwise it is a noise mode.

When noise reduction is performed for noise modes, the problem of signal oscillation due to discontinuity at the threshold for the hard thresholding function (HT) and signal distortion due to deviation between the original and estimated values of wavelet coefficients for the soft thresholding function (ST) are overcome. An improved wavelet threshold (IWT) function with a double modulation factor is proposed, whose expression is

$$\hat{w}_{j,k} = \begin{cases} sign\left(w_{j,k}\right)\left(\left|w_{j,k}\right| - \dfrac{(1-\alpha)\lambda}{2\beta+1}\right), \\ \quad \left|w_{j,k}\right| > \lambda \\ sign\left(w_{j,k}\right)\dfrac{(\alpha+2\beta)}{(2\beta+1)\lambda^{2\beta}}\left|w_{j,k}\right|^{2\beta+1}, \\ \quad \left|w_{j,k}\right| \leq \lambda \end{cases} \tag{9}$$

$$\lambda = \sigma\sqrt{2\log N} \tag{10}$$

where the parameters α and β are moderators, which are both positive; $w_{j,k}$ and $\hat{w}_{j,k}$ are the wavelet coefficients of the original signal before and after processing, respectively; *sign* is the step function; N is the signal length; λ is the threshold; and σ is the standard deviation of the noisy signal, where $\sigma = median\left(w_{j,k}\right)/0.6745$.

The procedure for proving the continuity and correlation of the improved threshold function is as follows.

The continuity analysis is

$$\lim_{w_{j,k}\to-\lambda^-} \hat{w}_{j,k} = \lim_{w_{j,k}\to-\lambda^+} \hat{w}_{j,k} = \frac{-(\alpha+2\beta)\lambda}{2\beta+1} \tag{11}$$

$$\lim_{w_{j,k}\to\lambda^-} \hat{w}_{j,k} = \lim_{w_{j,k}\to\lambda^+} \hat{w}_{j,k} = \frac{(\alpha+2\beta)\lambda}{2\beta+1} \tag{12}$$

This proves that the threshold function is continuous at the threshold, and thus overcomes the disadvantage that the hard threshold function curve is not continuous at the threshold.

The correlation analysis is

$$\lim_{w_{j,k}\to+\infty} \frac{\hat{w}_{j,k}}{w_{j,k}} = \lim_{w_{j,k}\to+\infty} \left(1 + \frac{(\alpha-1)\lambda}{(2\beta+1)w_{j,k}}\right) = 1 \tag{13}$$

$$\lim_{w_{j,k}\to-\infty} \frac{\hat{w}_{j,k}}{w_{j,k}} = \lim_{w_{j,k}\to-\infty} \left(1 + \frac{(1-\alpha)\lambda}{(2\beta+1)w_{j,k}}\right) = 1 \tag{14}$$

When $w_{j,k} \to \infty$, $\hat{w}_{j,k}$ approaches $w_{j,k}$ along the asymptote $\hat{w}_{j,k} = w_{j,k}$, which proves the correlation of the function. Thus, the bias between the original and estimated values of wavelet coefficients is reduced. The threshold function can be adjusted by adjusting the $\alpha\alpha$ and β parameters, which in turn changes the noise reduction performance.

C. HYBRID ENTROPY IN THE ULTRASONIC TIME-FREQUENCY DOMAIN

This paper proposes the concept of hybrid entropy in the time-frequency domain, which consists of fluctuation-based

dispersion entropy characterizing the signal amplitude change in the time domain and Hilbert marginal spectrum energy entropy characterizing the signal amplitude change in the frequency domain, so that the extracted characteristic information can fully reflect the characteristics of the sediment ultrasonic echo signal for both the time and frequency domains.

1) FLUCTUATION-BASED DISPERSION ENTROPY

The fluctuation-based dispersion entropy takes into account the differences in the dispersion patterns of neighbouring cells, which are sensitive to changes in synchronization frequency, amplitude and bandwidth. For a given time series $x = \{x_i, i = 1, 2, \ldots, N\}$. First, the normal cumulative distribution function (NCDF) is applied to map x to $y = \{y_i, i = 1, 2, \ldots, N\}$ in the range [0,1] and then a linear transformation is applied to assign y_i to the range [1,c], which is $z_j^c = round(c \cdot y_i + 0.5)$, where *round* is the rounding function and c is the number of categories. Then, the embedding vector $z_j^{m,c}$ is calculated according to $z_j^{m,c} = \left\{z_j^c, z_{j+d}^c, \ldots, z_{j+(m-1)d}^c\right\}, j = 1, 2, \ldots, N-(m-1)d$,where m and d are the embedding dimension and the time delay, respectively.

Next, map each embedding vector $z_j^{m,c}$ to a dispersion pattern $\pi_{v_0 v_1 \ldots v_{m-1}}$; the number of dispersion patterns assigned to each embedding vector $z_j^{m,c}$ is $(2c-1)^{m-1}$. For each dispersion pattern $\pi_{v_0 v_1 \ldots v_{m-1}}$, the relative frequency is obtained as follows:

$$p(\pi_{v_0 v_1 \ldots v_{m-1}}) = \frac{Number(\pi_{v_0 v_1 \ldots v_{m-1}})}{N-(m-1)d} \tag{15}$$

where $Number(\pi_{v_0 v_1 \ldots v_{m-1}})$ is the number of $z_j^{m,c}$ mapped to the dispersion pattern $\pi_{v_0 v_1 \ldots v_{m-1}}$.

Finally, based on Shannon's definition of entropy, the fluctuation-based dispersion entropy is calculated as follows:

$$FDispEn(x, m, c, d) = -\sum_{\pi}^{(2c-1)^{m-1}} p(\pi_{v_0 v_1 \ldots v_{m-1}}) \cdot \ln(p(\pi_{v_0 v_1 \ldots v_{m-1}})) \tag{16}$$

To obtain a robust fluctuation dispersion entropy, the number of categories c is set to 3 and the embedding dimension is set to 2.

2) HILBERT MARGINAL SPECTRUM ENERGY ENTROPY

The Hilbert marginal spectrum can characterize the amplitude change of the signal in the frequency domain, and the entropy value can effectively measure the slight change of the signal, so the energy entropy of the Hilbert marginal spectrum that can reflect the amplitude change of the signal in the whole frequency band is introduced. Calculating the Hilbert marginal spectrum energy values and normalizing them gives

$$p_k = E_k / \sum_{k=1}^{K} E_k \tag{17}$$

The Hilbert marginal spectrum energy entropy is further calculated as

$$H_k = -p_k \log p_k \tag{18}$$

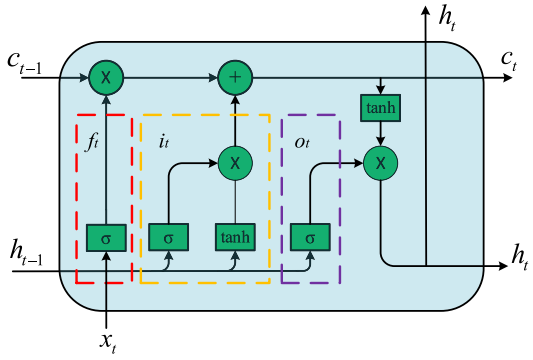

FIGURE 2. Basic structure of the LSTM. It mainly consists of a forgetting gate, an input gate, an output gate and a memory unit.

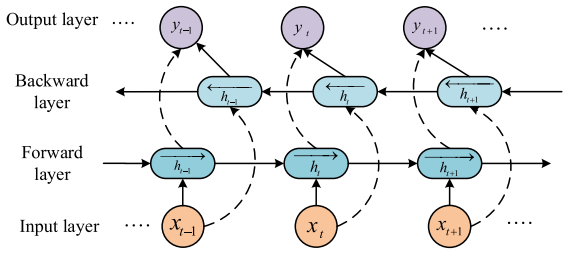

FIGURE 3. Basic structure of the Bi-LSTM. It mainly consists of an input layer, a forward layer, a backward layer, and an output layer.

where E_k and p_k are the energy value and energy normalized value of the kth IMF, respectively, and H_k is the Hilbert marginal spectrum energy entropy of the kth IMF.

D. INTELLIGENT IDENTIFICATION OF GRADING ELECTRODE SEDIMENT BASED ON MULTISCALE HYBRID ENTROPY IN THE TIME-FREQUENCY DOMAIN

Based on the above study, the multiscale hybrid entropy based on the time-frequency domain is used as the feature vector of the network model. The network model uses the Bi-LSTM network model, which is an improvement of the LSTM. The basic structure of the LSTM is shown in Figure 2; it mainly consists of a forgetting gate (f_t), an input gate (o_t), an output gate (i_t) and a memory unit (c_t). The 3 control gates allow for us to control the effect of the previous state of the system on the current output.

The compact formulation of the LSTM network is described as follows.

$$f_t = \sigma\left(W_f\left[h_{t-1}, x_t\right] + b_f\right) \tag{19}$$
$$i_t = \sigma\left(W_i\left[h_{t-1}, x_t\right] + b_i\right) \tag{20}$$
$$o_t = \sigma\left(W_o\left[h_{t-1}, x_t\right] + b_o\right) \tag{21}$$
$$\hat{C}_t = \tanh\left(W_C\left[h_{t-1}, x_t\right] + b_C\right) \tag{22}$$
$$C_t = f_t{}^* C_{t-1} + i_t{}^* \hat{C}_t \tag{23}$$
$$h_t = o_t{}^* \tanh\left(C_t\right) \tag{24}$$

where x_t represents the state of the input; h_t represents the final output of the memory unit; W_f, W_i, W_o, W_C represents the weight matrix; σ denotes the sigmoid function; $\hat{C}_t$ denotes the alternative vector required for the update; C_t denotes

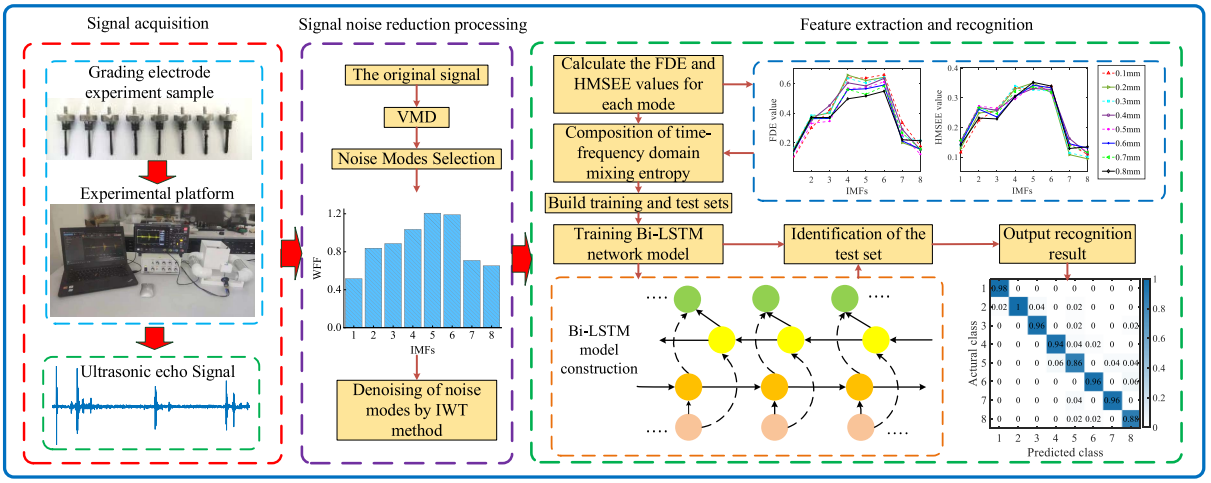

FIGURE 4. Feature extraction and intelligent recognition process of grading electrode sediment. Signal data is first obtained by experiment, then the signal is processed by noise reduction, and finally feature extraction and recognition is performed.

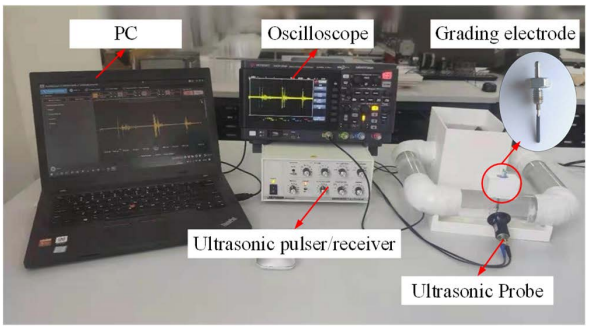

FIGURE 5. Experimental platform for grading electrode sediment detection. Ultrasonic pulser/receiver excites the ultrasonic probe to generate pulses to the object under test, and the ultrasonic probe receives the echo signal and transmits it back to the ultrasonic pulser/receiver, and then the echo signal is collected by the oscilloscope.

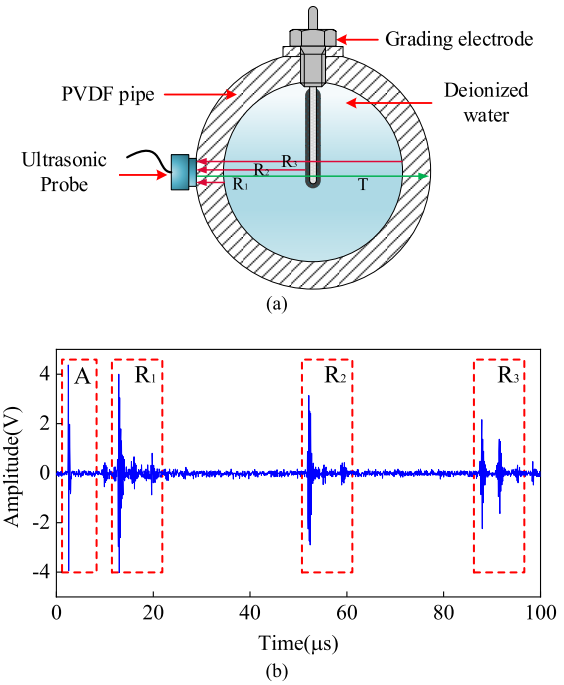

FIGURE 6. Ultrasound propagation in the pipe: (a) indicates the ultrasound propagation process, where T denotes the ultrasound propagation path, R_1 is the reflected echo signal at the inner tube wall-fluid interface, R_2 is the reflected echo signal at the grading electrode, R_3 is the reflected echo signal at the fluid-internal tube wall interface, and (b) indicates the acquired ultrasound echo signal, where A is the initial wave of the pulse.

the resulting new long-term memory; tanh is the activation function; and $*$ represents the dot product.

The Bi-LSTM network model considers both past and future information of the data, thus solving the problem that the LSTM does not utilize backward information. Its network structure is shown in Figure 3.

The network unit extracts the feature data in both directions simultaneously, and the output of the network unit at the current moment is

$$H_t = \left[\vec{h}_t, \overleftarrow{h}_t\right] \tag{25}$$

where $\overrightarrow{h}_t$ and $\overleftarrow{h}_t$ are the forward and backward outputs of the network unit at the current moment, respectively.

The intelligent identification process of grading electrode sediment is shown in Figure 4, and the specific steps as follows.

1. First, the echo signal data of the graded electrode sediment thickness in the range of 0.1 mm-0.8 mm were obtained experimentally.

2. Second, the signal is decomposed into k IMFs using the VMD, the weighted form factor index of each IMF is calculated, and the noise modes with an index less than 1 are preprocessed with the IWT method for noise reduction.

3. Third, the fluctuation-based dispersion entropy and Hilbert marginal spectrum energy entropy of each IMF after preprocessing are calculated according to Equations (16) and (18), respectively, and the hybrid entropy is characterized as the feature vector.

4. Finally, the sample data are divided into training and test sets, and the category labels of the graded electrode

sediment thickness are determined for the training and test sets. The training set is input to the Bi-LSTM network model for training and learning, the test set is input to the trained network to detect and identify the sediment condition of the grading electrode, and the identification results are output.

III. EXPERIMENTAL VALIDATION

A. EXPERIMENTAL PLATFORM AND DATA ACQUISITION

Referring to the arrangement of the ±500 kV converter valve cooling system and the grading electrode, a PVDF pipe with 60 mm outer diameter, 4 mm wall thickness was used as the converter valve convergence pipe. The experimental system is shown in Figure 5. The grading electrode was installed vertically in the centre of the pipe, and the electrode was inserted into the pipe at a depth of 28 mm. An Olympus D790-SM 5 MHz ultrasonic probe, JSR DPR300 ultrasonic pulse transmitter-receiver and oscilloscope were selected to detect the sediment condition in the tip area of the grading electrode. The specific testing process was as follows: an ultrasonic coupling agent was evenly applied to the tube wall, and the probe was firmly placed on the centre of the tube wall. The DPR300 excites the ultrasonic probe to generate pulses to the object under test, which generates reflected echoes at different media interfaces. The ultrasonic probe receives the echo signals and transmits them back to the DPR300, and the output of the DPR300 is connected to an oscilloscope for real-time echo signal acquisition.

The propagation path of ultrasound in the pipe and the real ultrasonic echo signal are shown in Figure 6, where echo A is the initial wave of the pulse, R_1 is the reflected echo signal at the inner tube wall-fluid interface, R_2 is the reflected echo signal at the grading electrode, and R_3 is the reflected echo signal at the fluid-internal tube wall interface. Due to the thin sediment layer on the surface of the grading electrode, a signal mixing phenomenon occurred, and the sediment layer thickness could not be obtained by calculation, so it was necessary to analyse the change in the sediment layer thickness by extracting signal features.

Using the experimental system above, the grading electrode with sediment thickness in the range of 0.1 mm-0.8 mm in the electrode tip area was divided into 8 grading electrode sediment thicknesses in steps of 0.1 mm. Under the same experimental conditions, echo signal data acquisition was performed for eight different sediment thicknesses of the grading electrodes. Two hundred sets of echo signal data were collected for each sediment thickness of the grading electrode samples, and a total of 1600 sets of sample data were acquired, with 2000 sampling points for each set of sample data.

To fully analyse the signal characteristics for both the time and frequency domains, 0.1 mm, 0.3 mm, 0.5 mm and 0.7 mm scale echo signals were selected for time domain analysis and smoothed pseudo-Wigner-Ville distribution (SPWVD) time frequency analysis.

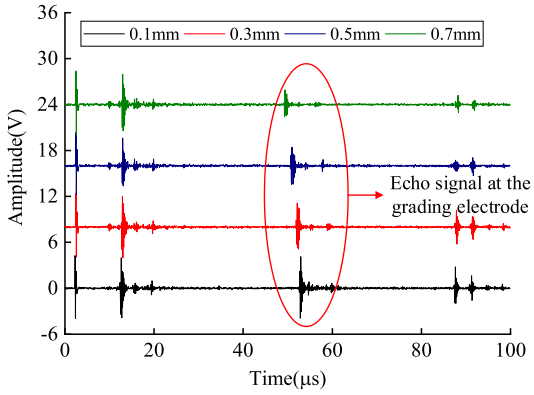

FIGURE 7. Time domain analysis of the echo signal. Echo signals of sediment thicknesses of 0.1 mm, 0.3 mm, 0.5 mm and 0.7 mm were selected, and it was found that the amplitude of the echo signal at the grading electrodes gradually decayed and the position gradually moved forward with the increase of the thickness of the grading electrode.

As shown in Figure 7, due to the attenuation characteristics of ultrasonic waves during of propagation, as the thickness of the grading electrode increases, the echo signal at the grading electrode gradually decays in amplitude and gradually moves forward in position.

The SPWVD time-frequency diagram is shown in Figure 8, and the effective signal frequency of the ultrasonic echo is mainly concentrated approximately 5 MHz. With the increase in the thickness of the grading electrode sediment, the echo signal amplitude and energy at the grading electrode decrease, and the ultrasonic echo signal amplitude and energy at the back wall decrease. As the ultrasonic wave propagates in the medium, it is scattered in the sediment layer, and thus an increase in thickness will increase the signal attenuation and scattering degree.

B. ENTROPY EXTRACTION AND FEATURE ENHANCEMENT

Extraction of the sediment signal feature vector is key to performing intelligent identification. Multiscale decomposition and noise mode selection were performed on the collected 1600 sets of sample data using the VMD-WFF algorithm, and the entropy features of each mode were extracted with the noise modes processed using noise-reduction methods to realize entropy feature enhancement.

First, the number of modal decompositions of VMD was determined using the centre frequency method. Taking the 0.3 mm sediment signal as an example, the centre frequencies corresponding to different values of k are shown in Table 1. When $k = 9$, the centre frequency values of the 6th and 7th modes are close to each other, and thus it is inferred that decomposition occurred, so the number of modes was determined.

Next, the noise modes of the signal were selected using the proposed weighted form factor index. The weighted form factor of each mode in Figure 9(a) was calculated and compared with the correlation coefficient and the weighted kurtosis index, and the comparison results are shown in Figure 10.

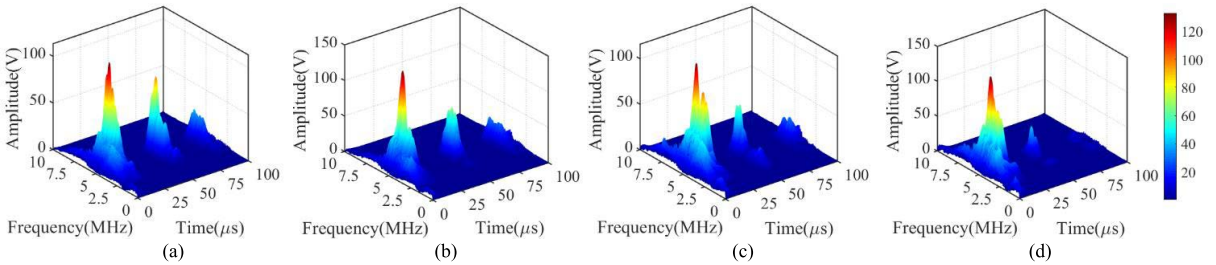

FIGURE 8. SPWVD analysis of the echo signal at different sediment thicknesses: (a) Thickness of 0.1 mm, (b) Thickness of 0.3 mm, (c) Thickness of 0.5 mm, and (d) Thickness of 0.7 mm. It was found that the amplitude and energy of the echo signal at the grading electrode decreased with the increase of the thickness of the grading electrode sediment.

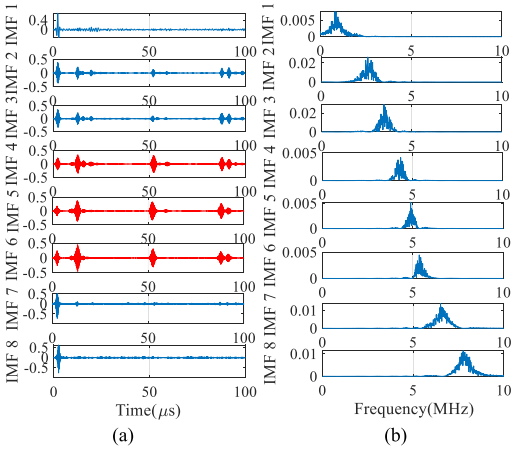

FIGURE 9. VMD decomposition of the 0.3 mm thickness sediment echo signal: (a) indicates the time domain diagram of each mode when the number of modes is eight, and (b) indicates the frequency domain diagram of each mode.

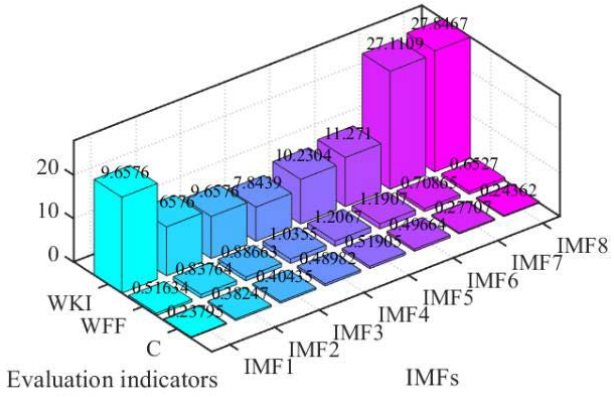

FIGURE 10. Comparison of different evaluation indicators. Effectiveness of the correlation coefficient method (C), the weighted kurtosis index (WKI) and the weighted form factor index (WFF) for the effective selection of noise modes was compared.

Combining Figure 9 with Figure 10, IMF4, IMF5 and IMF6 have high amplitudes, and the corresponding WFF indices are greater than 1, and the frequencies are all distributed around the effective signal frequency of 5 MHz, so they were judged to be effective modes, and the rest are noise modes.

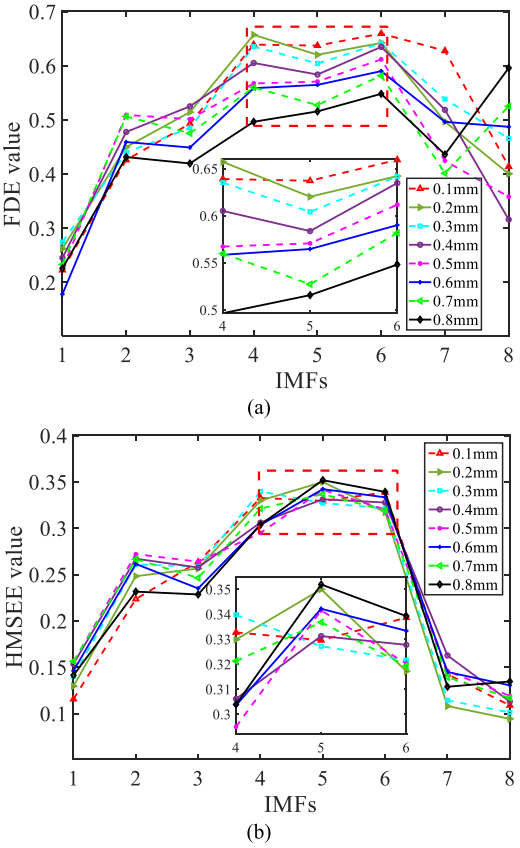

FIGURE 11. Entropy values of each mode without feature enhancement: (a) indicates the fluctuation-based dispersion entropy values, where the noise modes IMF7 and IMF8 have relatively high entropy values with irregular trends, and (b) indicates the Hilbert marginal spectrum energy entropy values, where the effective modes IMF4-IMF6 have an insignificant decreasing trend.

According to the correlation coefficient selection rules, the correlation coefficients range from $\pm 0.50 - \pm 0.80$ for significant correlation, and $\pm 0.80 - \pm 0.10$ for high correlation [44], only the IMF5 component has a correlation coefficient greater than 0.5, indicating that the single correlation coefficient method does not completely screen out the effective modes. While the WKI is susceptible to noise interference and is not sensitive to the effective modes of ultrasonic echo signals, the WFF index is more suitable for the identification of effective modes of ultrasonic echo signals than the other two methods.

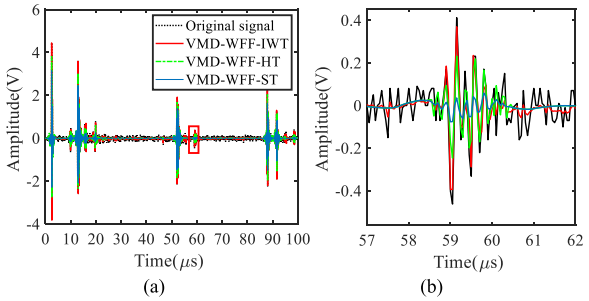

FIGURE 12. Comparison of the effects of different noise reduction methods: (a) indicates the comparison of the effects of signal noise reduction, and (b) indicates the partial amplification of the signal in the red box. It can be seen that the proposed VMD-WFF-IWT method retains the integrity of the signal compared with other methods.

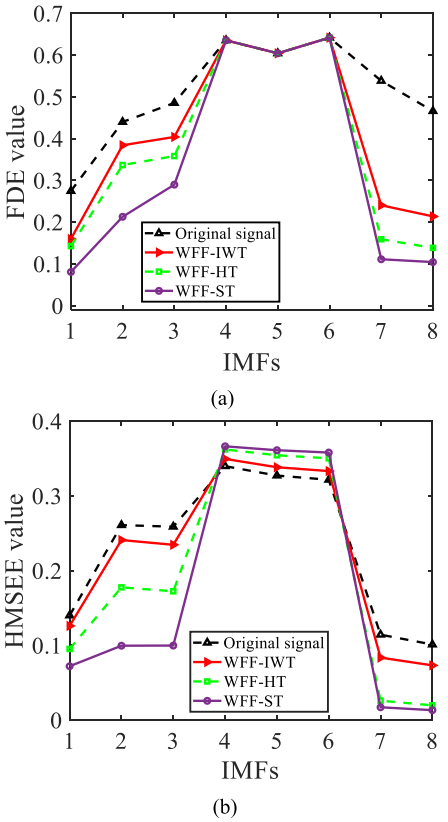

FIGURE 13. Comparison of the enhanced entropy features using different methods: (a) indicates the change in the fluctuation-based dispersion entropy, where the entropy values of the effective modes IMF4-IMF6 remain unchanged and the noise mode entropy values are weakened, and (b) indicates the change in the Hilbert marginal spectral energy entropy, where the entropy values of the effective modes IMF4-IMF6 are enhanced and the entropy values of the noise modes are weakened.

Then, VMD multiscale decomposition is performed on the echo signals of different sediment thicknesses and the entropy values of each mode are extracted. When the number of mode decompositions is $k = 8$, the entropy values of each mode for different sediment thickness signals are shown in Figure 11.

Figure 11 shows that the effective modes IMF4-IMF6 have a higher proportion of Hilbert marginal spectrum energy entropy values and fluctuation-based dispersion entropy values, and the noise mode energy entropy values are smaller.

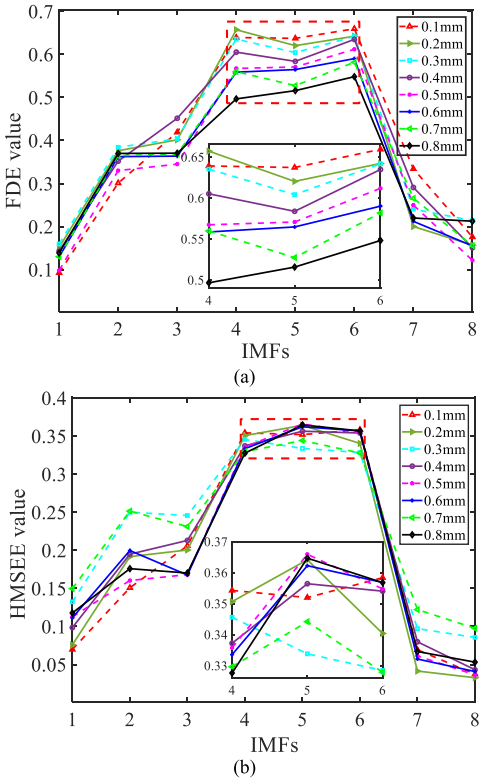

FIGURE 14. Entropy values of each mode after feature enhancement: (a) indicates the fluctuation-based dispersion entropy values, and (b) indicates the Hilbert marginal spectrum energy entropy values. It can be seen that the entropy value of the noise mode is significantly weakened, while the entropy value of the effective mode achieves enhancement.

As the sediment thickness increases, the decreasing trend of the fluctuation-based dispersion entropy values of the effective modes IMF4-IMF6 becomes more obvious, and can be used to effectively distinguish and reflect the change of the sediment thickness of the grading electrodes. However, the decreasing trend of the Hilbert marginal spectrum energy entropy values of the effective modes is not obvious due to the noise interference, and the fluctuation-based dispersion entropy values of the noise modes IMF7 and IMF8 are relatively high and the changing trend is irregular.

To enhance the entropy feature, the noise modes in Figure 9(a) were noise-reduced by the IWT method. A denoised signal was obtained by signal reconstruction, and a comparison of the effects of different noise reduction methods is shown in Figure 12. Through local magnification of the scaling at the homogenous electrode, it was found that the original signal is contaminated by noise and that the signal characteristic information is difficult to extract. Compared with the traditional noise reduction method, the proposed method preserves the signal integrity and effectively retains the characteristic information of the original signal.

The noise reduction index was used as the evaluation standard. The noise reduction indices $SNR = 15.1269$ and $RMSE = 0.0543$ obtained by the proposed IWT method are significantly better than the hard-threshold noise reduction

TABLE 1. Corresponding centre frequencies of each mode for different k values.

K	Centre frequencies (MHz)								
2	4.4434	5.4980	—	—	—	—	—	—	—
3	2.8906	4.4727	5.1367	—	—	—	—	—	—
4	3.1836	4.4627	5.1270	5.4297	—	—	—	—	—
5	2.8613	3.7598	4.4434	5.1953	5.6836	—	—	—	—
6	2.0312	3.4570	4.1602	4.8340	5.2734	8.5352	—	—	—
7	2.3047	3.1836	4.1699	4.7656	5.1270	5.5957	8.7012	—	—
8	0.8007	2.4707	3.7402	4.1504	4.7070	5.1660	5.5468	7.1777	—
9	0.9082	2.8906	3.4570	4.2676	4.7363	5.1270	5.3809	5.8008	8.5547

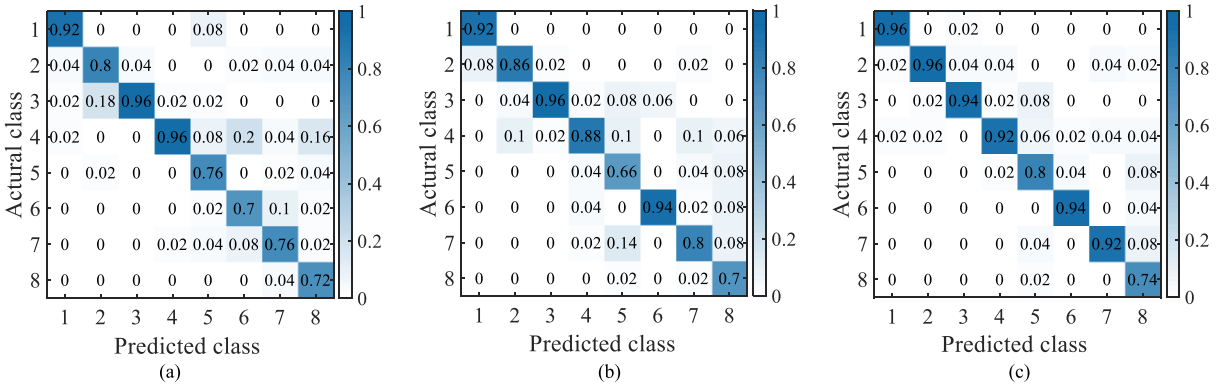

FIGURE 15. Confusion matrices for different input feature types under the "no feature enhancement" condition: (a) Fluctuation-based dispersion entropy, (b) Hilbert marginal spectrum energy entropy, and (c) Hybrid entropy. Using the hybrid entropy as feature vectors input to Bi-LSTM has higher recognition rate than entropy values in the time or frequency domain alone.

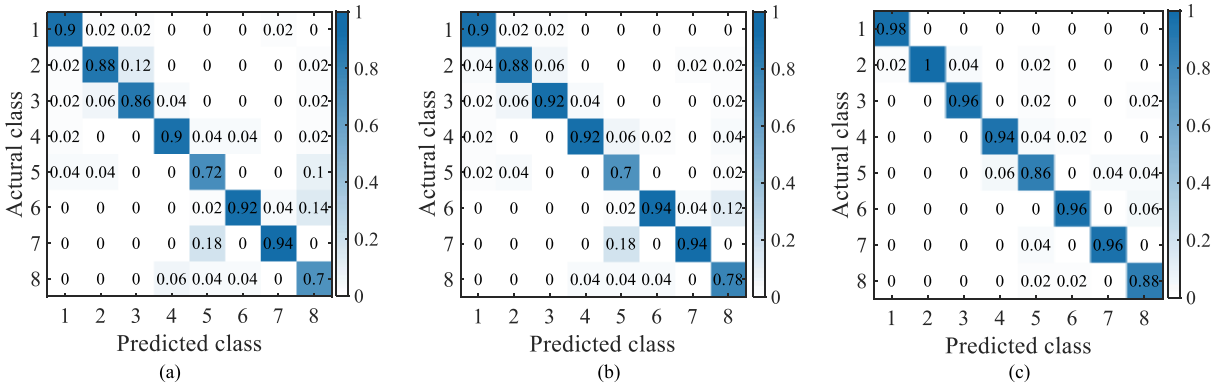

FIGURE 16. Confusion matrices for different input feature types under feature enhancement condition: (a) Fluctuation-based dispersion entropy, (b) Hilbert marginal spectrum energy entropy, and (c) Hybrid entropy. Entropy values after feature enhancement are input into Bi-LSTM has a higher recognition rate than that in Figure 15, where the hybrid entropy has a higher recognition rate than the entropy values in the time or frequency domain alone.

indices $SNR = 9.9403$ and $RMSE = 0.0987$, and the soft-threshold noise reduction indices $SNR = 7.5015$ and $RMSE = 0.1307$, showing a better noise reduction effect.

The fluctuation-based dispersion entropy and Hilbert marginal spectral energy entropy values of each mode were calculated and compared with the original signal entropy values as well as the entropy values obtained by other algorithms, and the results are shown in Figure 13.

The fluctuation-based dispersion entropy values of the effective modes IMF4-IMF6 remain unchanged and the noise mode entropy values are weakened, among which the noise mode entropy values of IMF7 and IMF8 decrease significantly. The Hilbert marginal spectral energy entropy values of effective modes IMF4-IMF6 are enhanced and the entropy values of the remaining noise modes are weakened. According to Equation (17), it can be seen that this is caused by the constant value of the effective mode energy and the decrease in the total energy value of the modes. Compared to the proposed IWT method, the entropy value obtained from noise modes after noise reduction by the conventional noise reduction method is diminished to a greater extent. This is due to the distortion of the signal caused by the conventional noise reduction method. Therefore, by processing the signal through the proposed VMD-WFF-IWT method and

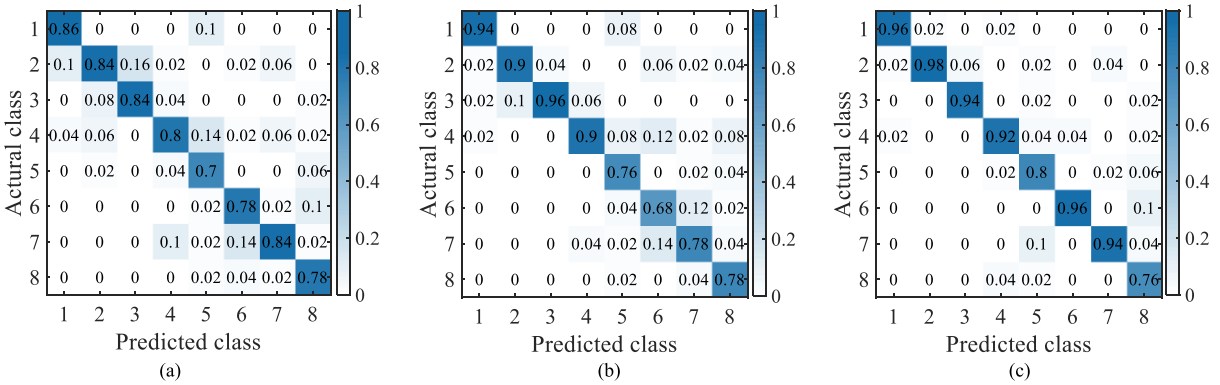

FIGURE 17. Confusion matrices of LSTM network under feature enhancement condition: (a) Fluctuation-based dispersion entropy, (b) Hilbert marginal spectrum energy entropy, and (c) Hybrid entropy. Entropy values after feature enhancement are input into LSTM has a lower recognition rate than Figure 16, where the hybrid entropy has a higher recognition rate than the entropy in the time or frequency domain alone.

then extracting the entropy values of each mode, the effective extraction of entropy values and the enhancement of entropy features can be achieved.

Figure 14 shows the results of entropy extraction of the echo signals with different sediment thicknesses using the VMD-WFF-IWT method. The entropy values of the noise modes are obviously weakened, and enhancement of the fluctuation-based dispersion entropy and Hilbert marginal spectrum energy entropy of the effective mode is realized. The entropy values of the effective modes show a decreasing trend as the sediment thickness increases. The fluctuation-based dispersion entropy and Hilbert marginal spectral energy entropy of each mode have obvious differences, which can reflect the sediment state of different thicknesses of grading electrodes on different scales, and can be used as feature vectors to distinguish the sediment state of grading electrodes.

C. INTELLIGENT IDENTIFICATION AND ANALYSIS OF GRADING ELECTRODE SEDIMENT

The features of the 1600 sets of data collected in the experiment were extracted with the above method, and the data were divided into a training set and a test set in a 3:1 ratio. In the identification process, eight types of classification labels with sediment thicknesses of 0.1 mm, 0.2 mm, 0.3 mm, 0.4 mm, 0.5 mm, 0.6 mm, 0.7 mm and 0.8 mm were set as 1, 2, 3, 4, 5, 6, 7 and 8 respectively.

The parameters of the Bi-LSTM network model were set as follows: segmentation window length $L = 50$, number of hidden layer nodes $S = 200$, and learning rate $\eta = 0.05$. To achieve better recognition, the network was gradient optimized using the Adam optimizer, the dropout technique was used to prevent overfitting, and the maximum number of iterations was set to 200.

To verify the recognition effect of the proposed method for different grading electrode sediment thicknesses, each entropy value without feature enhancement and with feature enhancement was input as a feature vector into the Bi-LSTM network model for training and recognition, respectively, and the corresponding confusion matrix outputs are shown in Figure 15 and Figure 16.

TABLE 2. Comparison of recognition accuracy of FDE, HMSEE and HE as feature vectors in lstm and bi-lstm classifiers, respectively.

Input feature type	Correct classification rate	
	LSTM classifier	Bi-LSTM classifier
FDE (Time domain)	80. 5%	85.25%
HMSEE (Frequency domain)	83.75%	87.25%
HE (Time-frequency domain)	90.75%	94.25%

From Figure 15 and Figure 16, it can be seen that the recognition rate of sediment thickness is low when the entropy values in time domain or frequency domain alone are used as the feature vector, and there is a problem that the recognition rate of a single class of sediment thickness is less than 80%. The recognition accuracy of all thicknesses is significantly improved after the two types of entropies were combined to comprise the hybrid entropy as the feature vector, and the recognition accuracy reached more than 80%. This indicates that the use of hybrid entropy as the feature vector results in a better recognition effect for the sediment thickness of the grading electrode. The recognition accuracy is further improved after the entropy feature enhancement, and the total recognition accuracy reached 94.25% when the feature-enhanced hybrid entropy was used as the feature vector, which further indicates that the multiscale hybrid entropy in the time-frequency domain processed by the VMD-WFF-IWT method is more effective for recognition of the grading electrode sediment thickness when used as the feature vector. It has a better recognition effect in the detection task of grading electrode sediment thickness in the range of 0.1 mm-0.8 mm.

To verify the advantages of the Bi-LSTM model over the LSTM model for recognition detection in this experiment, the hybrid entropy value under feature enhancement conditions was used as the feature vector and the LSTM network was

used for verification comparison, Figure 17 shows the recognition results of the LSTM model, and Table 2 shows the accuracy comparison of the two recognition models.

As seen from Figure 17 and Table 2, use of the hybrid entropy considering the time-frequency domain as the feature vector resulted in higher recognition accuracy compared with use of the time-domain or frequency-domain entropy features; the Bi-LSTM model can achieve better recognition results compared with the LSTM model.

IV. CONCLUSION

To realize the intelligent detection of grading electrode sediment in the converter valve cooling system of HVDC converter stations, this paper proposes an intelligent identification method for grading electrode sediment based on the multiscale hybrid entropy in the time-frequency domain and Bi-LSTM. A cooling system for the converter valve of the ±500 KV HVDC converter station was simulated and verified experimentally, and the following conclusions were drawn.

1) Multiscale hybrid entropy in the time-frequency domain is proposed to achieve multiscale characterization of the signal in the time-frequency domain, and the entropy is input into the Bi-LSTM network model as a feature vector for sediment thickness identification. The experimental results show that the proposed method has a good identification effect for the sediment thickness of the grading electrode in the range of 0.1 mm-0.8 mm, and the total identification accuracy reached 94.25%. The recognition effect of the model was better than that of the LSTM network model.

2) The weighted form factor index is proposed for the selection of noise modes of the ultrasonic echo signals, followed by extraction of their entropy values after noise reduction of the noise modes, for entropy value feature enhancement.

3) Use of the hybrid entropy in the time-frequency domain consisting of fluctuation-based dispersion entropy and Hilbert marginal spectral energy entropy as a feature vector is proposed, which can fully extract signal features from the time-frequency domain with a better recognition rate than the entropy value in the time or frequency domains alone.

Through the proposed method, the nondestructive detection and intelligent identification of the sediment of grading electrode are realized for the first time, which avoids the problem of equipment failure caused by the traditional manual detection method and is of great significance to the intelligent detection of the sediment of grading electrode.

In this paper, the optimization of the VMD decomposition parameters is performed by determining the mode number through a simple criterion of the centre frequency method and does not consider the optimization of the bandwidth control parameters, which is still a challenging problem. A potential solution is focused on optimizing the mode number and bandwidth control parameters by methods such as intelligent optimization algorithms and will be considered as a future work..

REFERENCES

[1] J. Li, L. Hao, F. Zheng, X. Chen, S. Wang, and Y. Fan, "Erosion corrosion behavior of aluminum electrode in simulated HVDC water cooling at 50 °C," *Int. J. Electrochem. Sci.*, vol. 15, no. 6, pp. 5320–5332, Jun. 2020.
[2] C. Wang, X. Liu, X. Wang, N. Liu, X. Jiao, and L. Liu, "Stray-current corrosion of aluminum heat sinks in different inner water cooling systems for HV converter valves," in *Proc. IEEE Electr. Insul. Conf. (EIC)*, Baltimore, MA, USA, Jun. 2017, pp. 400–403.
[3] C. Wang, X. Liu, X. Wang, N. Liu, X. Jiao, and L. Liu, "Effects of low electric current in deionized water dielectric on corrosion of aluminum heat sinks in HV converter valves," in *Proc. IEEE 19th Int. Conf. Dielectric Liquids (ICDL)*, Manchester, U.K., Jun. 2017.
[4] X. Wang, X. Liu, and C. Wang, "Research on mechanism and suppression of sediment deposition on grading electrodes in cooling water dielectric of HV converter valve," in *Proc. IEEE 3rd Int. Conf. Dielectr. (ICD)*, Valencia, Spain, Jul. 2020, pp. 293–296.
[5] X. Song, Y. Cheng, B. Gao, Y. Fan, T. He, and J. Ran, "Sediment deposition model of grading electrode in water cooling circuit of HVDC converter valve," *J. Eng.*, vol. 2019, no. 16, pp. 3396–3401, Mar. 2019.
[6] C. Wang, X. Liu, X. Wang, N. Liu, X. Jiao, and Y. Tan, "The distributing characteristics of sediment deposited on pin-type grading electrodes in inner cooling circuit of HV converter valve," in *Proc. IEEE Electr. Insul. Conf. (EIC)*, Seattle, WA, USA, Aug. 2015, pp. 24–28.
[7] Z. Yang, D. Li, X. Liu, B. Gong, X. Jiao, and S. Lu, "Research on the mechanism of sediment formation of Al compounds on platinum electrodes in inner water cooling systems for HVDC converter valves," *Int. J. Electrochem. Sci.*, vol. 16, no. 11, Nov. 2021, Art. no. 021129.
[8] S. Huang, H. Sun, L. Peng, S. Wang, Q. Wang, and W. Zhao, "Defect detection and identification of point-focusing shear-horizontal EMAT for plate inspection," *IEEE Trans. Instrum. Meas.*, vol. 70, 2021, Art. no. 9506409.
[9] Z. Fang and P. W. Tse, "Characteristics of spiral Lamb wave triggered by CL-MPT and its application to the detection of limited circumferential extent defects and axial extent evaluation within pipes," *IEEE Trans. Instrum. Meas.*, vol. 70, 2021, Art. no. 6008412.
[10] M. G. de Castro Ribeiro, A. C. Kubrusly, H. V. H. Ayala, and S. Dixon, "Machine learning-based corrosion-like defect estimation with shear-horizontal guided waves improved by mode separation," *IEEE Access*, vol. 9, pp. 40836–40849, 2021.
[11] T.-Y. Huang, J. Seo, and T. H. Chong, "Characterization of membrane wetting phenomenon by ionic liquid via ultrasonic time-domain reflectometry (UTDR)," *J. Membrane Sci.*, vol. 641, Jan. 2022, Art. no. 119949.
[12] X. Li, L. Sun, J. Li, and H. Piao, "Method for acquiring time of flight from high aliasing signal in heat exchange fouling ultrasonic testing," *Trans. Inst. Meas. Control*, vol. 43, no. 11, pp. 2438–2449, Jul. 2021.
[13] L. Lai, L. N. Sim, W. B. Krantz, and T. H. Chong, "Characterization of colloidal fouling in forward osmosis via ultrasonic time- (UTDR) and frequency-domain reflectometry (UFDR)," *J. Membrane Sci.*, vol. 602, May 2020, Art. no. 117969.
[14] M. Yang, X. Li, L. Sun, and X. Zhao, "Research of heat exchanger fouling ultrasonic testing signal analysis method based on inverse filtering and high order cumulant MUSIC spectrum estimation," in *Proc. IEEE Int. Conf. Autom. Logistics*, Zhengzhou, China, Aug. 2012, pp. 563–566.
[15] Y. Song, X. Zi, Y. Fu, X. Li, C. Chen, and K. Zhou, "Nondestructive testing of additively manufactured material based on ultrasonic scattering measurement," *Measurement*, vol. 118, pp. 105–112, Mar. 2018.
[16] Y. Song, J. A. Turner, Z. Peng, C. Chen, and X. Li, "Enhanced ultrasonic flaw detection using an ultrahigh gain and time-dependent threshold," *IEEE Trans. Ultrason., Ferroelectr., Freq. Control*, vol. 65, no. 7, pp. 1214–1225, Jul. 2018.
[17] X. Wang, S. Si, and Y. Li, "Multiscale diversity entropy: A novel dynamical measure for fault diagnosis of rotating machinery," *IEEE Trans. Ind. Informat.*, vol. 17, no. 8, pp. 5419–5429, Aug. 2021.
[18] Z. Huo, M. Martinez-Garcia, Y. Zhang, R. Yan, and L. Shu, "Entropy measures in machine fault diagnosis: Insights and applications," *IEEE Trans. Instrum. Meas.*, vol. 69, no. 6, pp. 2607–2620, Jun. 2020.
[19] H. Cui, Q. Liu, J. Zhang, and B. Kang, "An improved Deng entropy and its application in pattern recognition," *IEEE Access*, vol. 7, pp. 18284–18292, 2019.
[20] Y. Kumar, M. Dewal, and R. Anand, "Epileptic seizure detection using DWT based fuzzy approximate entropy and support vector machine," *Neurocomputing*, vol. 133, pp. 271–279, Jun. 2014.

[21] W. Feng, X. Zhou, X. Zeng, and C. Yang, "Ultrasonic flaw echo enhancement based on empirical mode decomposition," *Sensors*, vol. 19, no. 2, p. 236, Jan. 2019.
[22] D. Pellicano, I. Palamara, M. Cacciola, S. Calcagno, M. Versaci, and F. C. Morabito, "Fuzzy similarity measures for detection and classification of defects in CFRP," *IEEE Trans. Ultrason., Ferroelectr, Freq. Control*, vol. 60, no. 9, pp. 1917–1927, Sep. 2013.
[23] H. Liu and M. Han, "A fault diagnosis method based on local mean decomposition and multi-scale entropy for roller bearings," *Mech. Mach. Theory*, vol. 75, pp. 67–78, May 2014.
[24] J. Chang, C. Zheng, and Q.-Q. Ni, "The ultrasonic wave propagation in composite material and its characteristic evaluation," *Compos. Struct.*, vol. 75, nos. 1–4, pp. 451–456, 2006.
[25] D. Datta and N. N. Kishore, "Features of ultrasonic wave propagation to identify defects in composite materials modelled by finite element method," *NDT & E Int.*, vol. 29, no. 4, pp. 213–223, Aug. 1996.
[26] G. Zhang, X. Li, S. Zhang, and T. Kundu, "Investigation of frequency-dependent attenuation coefficients for multiple solids using a reliable pulse-echo ultrasonic measurement technique," *Measurement*, vol. 177, Jun. 2021, Art. no. 109270.
[27] H. Azami and J. Escudero, "Amplitude- and fluctuation-based dispersion entropy," *Entropy*, vol. 20, no. 3, p. 210, Mar. 2018.
[28] Y. Ke, C. Yao, E. Song, Q. Dong, and L. Yang, "An early fault diagnosis method of common-rail injector based on improved CYCBD and hierarchical fluctuation dispersion entropy," *Digit. Signal Process.*, vol. 114, Jul. 2021, Art. no. 103049.
[29] X. L. Li, D. Li, Z. H. Liang, L. J. Voss, and J. W. Sleigh, "Analysis of depth of anesthesia with Hilbert–Huang spectral entropy," *Clin. Neurophysiol.*, vol. 119, no. 11, pp. 2465–2475, Nov. 2008.
[30] Q. Yang, J. Ruan, Z. Zhuang, and D. Huang, "Fault identification for circuit breakers based on vibration measurements," *IEEE Trans. Instrum. Meas.*, vol. 69, no. 7, pp. 4154–4164, Jul. 2020.
[31] M. Costa, A. L. Goldberger, and C.-K. Peng, "Multiscale entropy analysis of complex physiologic time series," *Phys. Rev. Lett.*, vol. 89, no. 6, Jul. 2002, 068102.
[32] W. Aziz and M. Arif, "Multiscale permutation entropy of physiological time series," in *Proc. Pakistan Sect. Multitopic Conf.*, Karachi, Pakistan, Dec. 2005, pp. 368–373.
[33] X. Y. Ji, H. L. Wang, Y. T. Ge, J. T. Liang, and X. L. Xu, "Empirical mode decomposition-refined composite multiscale dispersion entropy analysis and its application to geophysical well log data," *J. Petroleum Sci. Eng.*, vol. 208, Jan. 2022, Art. no. 109495.
[34] X. P. Xie, W. D. Chen, B. G. Chen, J. S. Cheng, and L. G. Tan, "Comprehensive fatigue estimation and fault diagnosis based on refined generalized multi-scale entropy method of centrifugal fan blades," *Measurement*, vol. 166, Dec. 2020, Art. no. 108224.
[35] K. Dragomiretskiy and D. Zosso, "Variational mode decomposition," *IEEE Trans. Signal Process.*, vol. 62, no. 3, pp. 531–544, Feb. 2014.
[36] Q. Ni, J. C. Ji, K. Feng, and B. Halkon, "A fault information-guided variational mode decomposition (FIVMD) method for rolling element bearings diagnosis," *Mech. Syst. Signal Process.*, vol. 164, Feb. 2022, Art. no. 108216.
[37] Q. Huang, L. Xie, G. Yin, M. Ran, X. Liu, and J. Zheng, "Acoustic signal analysis for detecting defects inside an arc magnet using a combination of variational mode decomposition and beetle antennae search," *ISA Trans.*, vol. 102, pp. 347–364, Jul. 2020.
[38] Y. Liu, G. Yang, M. Li, and H. Yin, "Variational mode decomposition denoising combined the detrended fluctuation analysis," *Signal Process.*, vol. 125, pp. 349–364, Aug. 2016.
[39] Z. Li, J. Chen, Y. Zi, and J. Pan, "Independence-oriented VMD to identify fault feature for wheel set bearing fault diagnosis of high speed locomotive," *Mech. Syst. Signal Process.*, vol. 85, pp. 512–529, Feb. 2017.
[40] Y. Lv, R. Yuan, and G. Song, "Multivariate empirical mode decomposition and its application to fault diagnosis of rolling bearing," *Mech. Syst. Signal Process.*, vol. 81, pp. 219–234, Dec. 2016.
[41] Y. Zhang, Y. Lv, and M. Ge, "Time–frequency analysis via complementary ensemble adaptive local iterative filtering and enhanced maximum correlation kurtosis deconvolution for wind turbine fault diagnosis," *Energy Rep.*, vol. 7, pp. 2418–2435, Nov. 2021.
[42] X. Zhang, Q. Miao, H. Zhang, and L. Wang, "A parameter-adaptive VMD method based on grasshopper optimization algorithm to analyze vibration signals from rotating machinery," *Mech. Syst. Signal Process.*, vol. 108, pp. 58–72, Aug. 2018.
[43] G. Bing, T. He, Y. Fan, L. Chao, X. Song, and Y. Cheng, "Investigation on deposition behavior of HVDC water cooling system based on electro-mass transfer-velocity coupling model," *IEEE Access*, vol. 7, pp. 67960–67971, 2019.
[44] A. G. Asuero, A. Sayago, and A. González, "The correlation coefficient: An overview," *Crit. Rev. Anal. Chem.*, vol. 36, no. 1, pp. 41–59, 2006.

WEIHUA CHEN was born in Heilongjiang, China, in 1980. He received the master's and Ph.D. degrees from Liaoning Technical University, in 2006 and 2016, respectively.

He is currently an Associate Professor at Liaoning Technical University. His research interests include electromagnetic ultrasound detection and wireless energy transmission technology.

HONGQIANG CHEN was born in Shandong, China, in 1995. He is currently pursuing the master's degree with Liaoning Technical University. His research interest includes ultrasonic nondestructive testing.

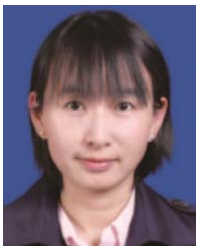

XIAOHENG YAN was born in Liaoning, China, in 1984. She received the master's and Ph.D. degrees from Liaoning Technical University, in 2008 and 2016, respectively.

She is currently an Associate Professor at Liaoning Technical University. Her research interests include electromagnetic ultrasound detection and imaging, and biomedical imaging.

YANJU YANG was born in Hebei, China, in 1985. She received the master's degree from North China Electric Power University, in 2012, and the Ph.D. degree from the Institute of Electrical Engineering, Chinese Academy of Sciences, in 2017.

She is currently an Associate Professor at the Chongqing University of Arts and Sciences. Her research interests include engineering electromagnetic field and intelligent detection technology.

SHIWEI JIN was born in Liaoning, China, in 1990. He received the master's degree from Liaoning Technical University, in 2019.

He is currently a Mid-Level Engineer at the Maintenance Branch, State Grid Liaoning Electric Power Company.